

# End-to-End Out-of-distribution Detection with Self-supervised Sampling

Sen Pei<sup>1,2</sup>, Jiayi Sun<sup>2</sup>, Peng Qin<sup>3</sup>, Qi Chen<sup>1</sup>, Xinglong Wu<sup>1</sup>, Xun Wang<sup>1\*</sup>

<sup>1</sup> ByteDance Inc.

<sup>2</sup> NLPR, Institute of Automation, Chinese Academy of Sciences

<sup>3</sup> Sun Yat-sen University

{peisen,wangxun.2}@bytedance.com

## Abstract

Out-of-distribution (OOD) detection empowers the model trained on the closed set to identify unknown data in the open world. Though many prior techniques have yielded considerable improvements, two crucial obstacles still remain. Firstly, a unified perspective has yet to be presented to view the developed arts with individual designs, which is vital for providing insights into the related directions. Secondly, most research focuses on the post-processing schemes of the pre-trained features while disregarding the superiority of end-to-end training, dramatically limiting the upper bound of OOD detection. To tackle these issues, we propose a general probabilistic framework to interpret many existing methods and an OOD-data-free model, namely Self-supervised Sampling for OOD Detection (SSOD), to unfold the potential of end-to-end learning. SSOD efficiently exploits natural OOD signals from the in-distribution (ID) data based on the local property of convolution. With these supervisions, it jointly optimizes the OOD detection and conventional ID classification. Extensive experiments reveal that SSOD establishes competitive state-of-the-art performance on many large-scale benchmarks, where it outperforms the most recent approaches, such as KNN [Sun et al., 2022], by a large margin, e.g., **48.99% → 35.52%** on *SUN* at FPR95.

## 1 Introduction

Out-of-distribution (OOD) detection has been recognized as crucial for the deployment of machine learning systems in reality, *e.g.*, computer vision applications. Traditional neural networks excel at handling in-distribution (ID) data, which is similar to the training samples. However, real-world scenarios cannot always adhere to the independent and identically distributed rules, *i.e.*, the *i.i.d.* conditions. That means the input data can vary significantly from the training images in terms of domains and categories. Thus, extensive efforts have been devoted to detecting whether input samples are OOD, ultimately bolstering classifier stability and reliability.

Current OOD detection methods primarily rely on the perspective of statistical difference, *i.e.*, observing distinctions between the pre-trained features of ID/OOD samples. These methods tend to use heuristic tricks to rule out OOD data in a two-stage manner, *i.e.*, pre-training and post-processing, which suffer from the following drawbacks compared to the end-to-end fashion. Firstly, the frozen model weights are obtained on the ID classification task with limited OOD supervision, and therefore, the extracted features inherently carry bias which is not distinguishable enough for identifying OOD data (cf. Figure 2). Secondly, the two-stage design yields poor scalability and efficiency since it is not suitable for scenarios without pre-trained models, *e.g.*, given a practical application and its

---

\*Corresponding Author

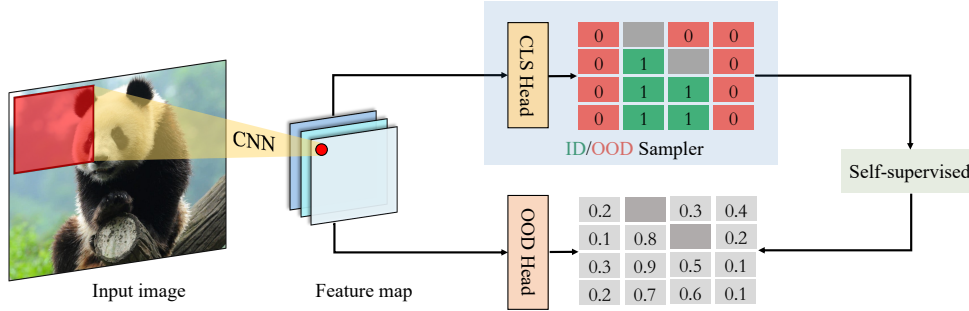


Figure 1: Self-supervised Sampling for Out-of-distribution Detection (SSOD). We adopt a self-supervised sampling scheme to train the OOD discrimination branch, *i.e.*, the OOD head with the supervised signals injected by the CLS head. The image blocks in green/red/gray are ID/OOD/invalid signals identified by the CLS head. SSOD jointly trains these two branches.

corresponding dataset, a two-stage model takes comparable training tax compared to the end-to-end method while only obtaining biased features and fair to good detection results.

To tackle the issues above, this paper interprets the OOD detection task with a unified probabilistic framework (cf. Section 3), which can include many previous individual designs widely. To be concrete, our framework divides the multi-category classification problem into two tasks: conventional ID classification and OOD detection. According to the theoretical analysis, the deficiency encountered by traditional neural networks in identifying OOD data arises from the absence of a critical component, *i.e.*, an OOD factor that estimates the likelihood of images belonging to the in-distribution. Furthermore, sailing from this general foundation, we present **Self-supervised Sampling for OOD Detection (SSOD)**, an end-to-end trainable framework **w/o** resorting to explicit OOD annotations (cf. Section 4). In contrast to the observed paths that hug synthetic OOD features, SSOD directly samples **real** OOD supervision from the background of training images by itself, *i.e.*, self-supervised, getting rid of the constraints resulted by the lack of labeled OOD data and the deviation introduced within the OOD feature syntheses stage. Extensive experiments demonstrate that the jointly end-to-end training manner significantly improves the OOD detection performance and guides the model to focus more on the object-discriminative characters instead of the meaningless background information (cf. Figure 3). The major contributions of this paper are summarized as follows.

- We establish a general probabilistic framework to interpret the OOD detection, where various OOD methods can be analyzed comprehensively, with main differences and key limitations clearly identified.
- To mitigate the negative impacts from pre-trained features, we design an end-to-end trainable model, namely **Self-supervised Sampling for OOD Detection (SSOD)**, to sample real OOD signals from the ID images. SSOD can avoid the labor-intensive work of labeling/cleaning sufficient OOD images.
- SSOD is evaluated across various benchmarks and model architectures for OOD detection, where it outperforms current state-of-the-art approaches by a large margin, *e.g.*, improving KNN [Sun et al., 2022] w/ and w/o contrastive learning with -17.71% and -21.97% FPR95 on Places [Zhou et al., 2018], and Energy [Liu et al., 2020] with +2.01% AUROC and -15.10% FPR95 on SUN [Xiao et al., 2010]. The scalability and superiority of SSOD promise its potential to be a starting point for solving the OOD detection problem.

## 2 Related work

We give a brief overview of the observed paths in promoting the detection of OOD data.

**Score-based posterior calibration.** This line of research aims to find differences between the ID and OOD data, thus designing model-specific discriminative functions to identify the OOD samples. The related work includes ODIN [Liang et al., 2018], LogitNorm [Wei et al., 2022], GradNorm [Huang et al., 2021], ReAct [Sun et al., 2021], Energy [Liu et al., 2020], and CIDER [Ming et al., 2023], to name a few. Generally, these methods are usually pre- or post-processing schemes that demonstrate

no need for retraining the neural networks. Although these methods above report considerable performance improvements and sometimes are training efficient, they do not necessarily lead to significant generalization ability. For example, ReAct [Sun et al., 2021] investigates the distinct behaviors of ID and OOD data after ReLU function, and therefore, it fails to perform on architectures adopting other activations, such as GELU, Sigmoid, and Tanh, *etc.* Similarly, the ODIN [Liang et al., 2018] investigates post-processing schemes specially designed for Softmax, *i.e.*, the temperature scaling. These specific designs promote OOD detection but limit the model’s scalability. In contrast, our SSOD doesn’t suffer from this limitation as it addresses the OOD detection directed by Bayes’ theorem, which holds in general scenarios.

**Auxiliary supervision from synthetic OOD data.** The lack of OOD supervision is a critical factor leading to unsatisfactory performance in OOD detection. Thus, significant interest has been raised in generating synthetic OOD data. Existing approaches tackling this issue can be roughly divided into two manners, which are feature and image generation. The feature generation manner samples OOD features from the ID boundary, such as VOS [Du et al., 2022], or generates them using GAN, such as BAL [Pei et al., 2022]. In contrast, the image generation yields more expensive training tax since it directly generates the OOD images, such as Conf [Lee et al., 2018a], SBO [Möller et al., 2021], MG-GAN [Dendorfer et al., 2021], NAS-OOD [Bai et al., 2021], CODEs [Tang et al., 2021], and VITA [Chen et al., 2022], *etc.* In summary, existing methods either employ unrealistic OOD supervision as they only consider the approximated feature space or are costly due to the generation in the original image space. Unlike prior arts, our proposed SSOD avoids both limitations by utilizing the universal local property of neural networks, extracting realistic OOD supervision from the ID images without generation cost.

### 3 Probabilistic framework for OOD detection

In this section, we first introduce the unified probabilistic OOD framework and then revisit existing OOD detection methods from the view.

#### 3.1 Probabilistic OOD detection

The problem of OOD detection can be defined in various ways. In this paper, we formalize the task as a binary classification problem. Concretely, we consider two **disjoint** distributions on the data and label space, denoted as  $\mathcal{S}_{\text{ID}} \times \mathcal{Y}_{\text{ID}}$  and  $\mathcal{S}_{\text{OOD}} \times \mathcal{Y}_{\text{OOD}}$ , representing the ID distribution and OOD distribution respectively. We note that  $\mathcal{Y}_{\text{ID}}$  and  $\mathcal{Y}_{\text{OOD}}$  have no overlap, *i.e.*,  $\mathcal{Y}_{\text{ID}} \cap \mathcal{Y}_{\text{OOD}} = \emptyset$ . OOD detection aims to train a model, which can effectively distinguish the source distribution of a given image  $x$ . Moreover, for  $x \in \mathcal{S}_{\text{ID}} \times \mathcal{Y}_{\text{ID}}$ , it is also expected to correctly predict its corresponding category with a classifier denoted as  $f(\cdot)$ .

Supposing  $x$  is a given image sampled from the open image distribution  $\mathcal{S} = \mathcal{S}_{\text{ID}} \cup \mathcal{S}_{\text{OOD}}$ , and  $\mathcal{W}_1, \mathcal{W}_2, \dots, \mathcal{W}_M$  are the sets of the  $M$  ID categories, we can obtain the following formula to compute  $P(x \in \mathcal{W}_i | x \in \mathcal{S})$  based on the law of total probability,

$$P(x \in \mathcal{W}_i | x \in \mathcal{S}_{\text{ID}})P(x \in \mathcal{S}_{\text{ID}} | x \in \mathcal{S}) + P(x \in \mathcal{W}_i | x \in \mathcal{S}_{\text{OOD}})P(x \in \mathcal{S}_{\text{OOD}} | x \in \mathcal{S}). \quad (1)$$

As  $P(x \in \mathcal{W}_i | x \in \mathcal{S}_{\text{OOD}}) = 0$ , Eqn.(1) leads to a practical conclusion:

$$P(x \in \mathcal{W}_i | x \in \mathcal{S}) \triangleq P(x \in \mathcal{W}_i | x \in \mathcal{S}_{\text{ID}})P(x \in \mathcal{S}_{\text{ID}} | x \in \mathcal{S}), \quad (2)$$

where  $\triangleq$  indicates the conditional equation. The conditional probability  $P(x \in \mathcal{W}_i | x \in \mathcal{S}_{\text{ID}})$  in Eqn.(2) is exactly the classification problem of ID data, termed as **ID factor**.  $P(x \in \mathcal{S}_{\text{ID}})$ , namely **OOD factor**, is the OOD detection task. Generally, OOD detection techniques aim to optimize the OOD factor without affecting the ID classification performance.

#### 3.2 Revisit OOD methods with the probabilistic view

We interpret several classic OOD detection techniques from the perspective of our proposed probabilistic framework and find that most OOD detection methods hold  $P(x \in \mathcal{W}_i | x \in \mathcal{S}_{\text{ID}}) = f_i(x)$ , *i.e.*, the  $i$ -th dimension of the classifier’s output activated by Softmax function. Thus, the crucial point is how to compute the OOD factor  $P(x \in \mathcal{S}_{\text{ID}} | x \in \mathcal{S})$ .

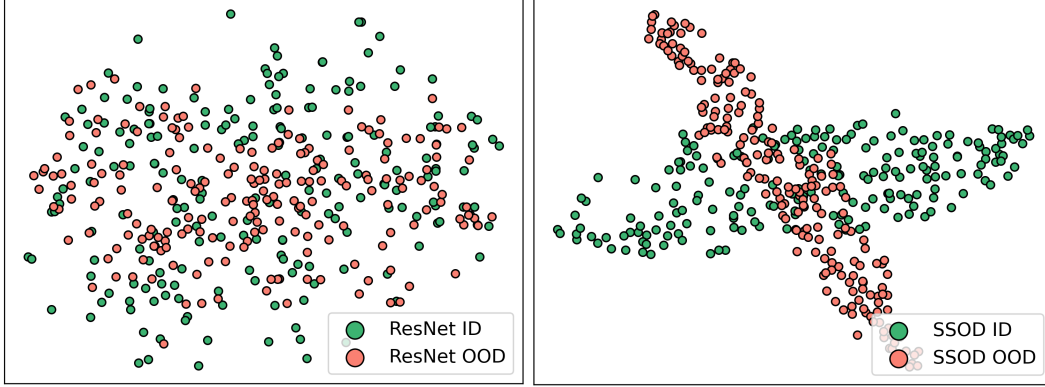


Figure 2: The t-SNE visualizations of deep features for the iNaturalist dataset. **Left:** features extracted by the conventional ResNet-50. **Right:** features extracted by our SSOD. The green/red dots represent ID/OOD features, *i.e.*, the ImageNet/iNaturalist. SSOD improves the feature’s ID/OOD discriminability notably. The overlap of ID/OOD features reflects the false positive rate (FPR).

**Methods based on logits**, *e.g.*, Max-Softmax Probability (MSP) [Hendrycks, 2017], which directly employs the Softmax output of classifiers as the ID/OOD score, aiming to distinguish them with classification confidence. Concretely, given image  $x$ , MSP uses the following expressions to depict the procedure of OOD detection:

$$x \rightarrow f(\cdot) \rightarrow \begin{cases} x \in \mathcal{S}_{\text{OOD}}, & \max f(x) < \gamma \\ x \in \mathcal{S}_{\text{ID}}, & \max f(x) \geq \gamma \end{cases}. \quad (3)$$

Intuitively, MSP expects the classifier  $f(\cdot)$  to assign higher confidence, *i.e.*,  $\max f(x)$  to ID samples and lower of that to the OOD. Obviously, for MSP, the OOD factor is built as follows:

$$P(x \in \mathcal{S}_{\text{ID}} | x \in \mathcal{S}) = P(\max f(x) \geq \gamma). \quad (4)$$

**Methods based on features** try to distinguish ID/OOD based on their deep features extracted by the backbone termed as  $h(\cdot)$ , including ReAct [Sun et al., 2021], BAL [Pei et al., 2022], VOS [Du et al., 2022], and KNN [Sun et al., 2022], *etc.* Taking ReAct as an example, it builds the OOD factor  $P(x \in \mathcal{S}_{\text{ID}})$  in a hard threshold manner with linear projection, depicted as:

$$P(x \in \mathcal{S}_{\text{ID}} | x \in \mathcal{S}) = P(\mathbf{W}^\top \text{ReAct}(h(x), c) + \mathbf{b} \geq \gamma), \quad (5)$$

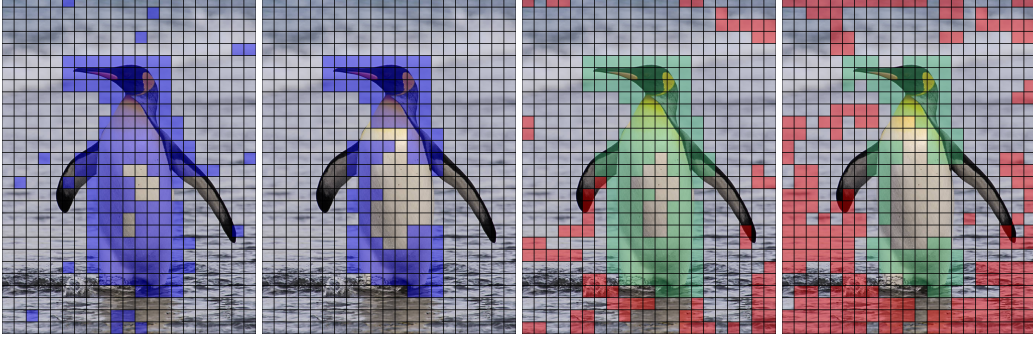
where  $\mathbf{W}^\top$  and  $\mathbf{b}$  are the weight matrix and bias vector,  $\text{ReAct}(h(x), c) = \min\{h(x), c\}$  is an element-wise truncation function, and  $\gamma$  is a hard threshold. Instead of the OOD-syntheses-free schemes like ReAct and KNN, BAL and VOS generate ID/OOD supervision in the feature space to optimize the ID/OOD classifier with  $P(x \in \mathcal{S}_{\text{ID}} | x \in \mathcal{S}) = \sigma(d(h(x)))$ , where  $d(\cdot)$  is a discriminator.

In summary, most OOD methods approximate the OOD factor  $P(x \in \mathcal{S}_{\text{ID}} | x \in \mathcal{S})$  by  $P(f(x) \in f(\mathcal{S}_{\text{ID}}) | f(x) \in f(\mathcal{S}))$  as MSP, or  $P(h(x) \in h(\mathcal{S}_{\text{ID}}) | h(x) \in h(\mathcal{S}))$  like ReAct, BAL, VOS, and KNN. We note here that  $f(x)$  is the Softmax output, and  $h(x)$  is the feature extracted by the backbone. Nevertheless, there is a significant bias introduced in  $f(\mathcal{S})$  and  $h(\mathcal{S})$  as  $f(\cdot)$  and  $h(\cdot)$  are trained for the ID classification. It adversely affects the discrimination of ID and OOD data (cf. Figure 2, left). Furthermore, generated OOD signals in the feature space (*e.g.*, BAL and VOS) do not necessarily lead to the existence of a corresponding natural OOD image. Consequently, its effectiveness in practical scenarios of the open world may be limited. To remove these obstacles, we propose to *sample OOD supervision from the ID images and optimize the OOD factor directly*.

## 4 Self-supervised Sampling for OOD Detection (SSOD)

In this section, we propose a Self-supervised Sampling solution to tackle OOD Detection problem, termed as **SSOD**, which can estimate the OOD factor directly without resorting to explicit OOD samples. The design of SSOD is inspired by the local property, *i.e.*, *locality*<sup>2</sup>, from convolution networks, as discussed below.

<sup>2</sup>In this paper, ‘locality’ represents the local property.



(a) Locality of ResNet-50. (b) Locality of SSOD. (c) Samplers of ResNet-50. (d) Samplers of SSOD.

Figure 3: **(a)**: The image blocks in **blue** are recognized as penguins with over 40% confidence by the vallina ResNet-50 classifier. **(b)**: The SSOD counterpart of (a). **(c)**: The image blocks in **green** and **red** are sampled as ID and OOD supervision with over 95% confidence by ResNet. **(d)**: The SSOD counterpart of (c). It is noteworthy that SSOD is motivated by the local property of conventional networks as illustrated in (a), and the results depicted in (b) reveal that the local property is enhanced by the joint training.

#### 4.1 Inspiration of SSOD

Prior studies, *e.g.*, Redmon et al. [2016] and Carion et al. [2020], have demonstrated that traditional neural networks are capable of retaining spatial information. Specifically, a position of the feature map reflects the corresponding position in the input image. Thus, we may expect the potential to extract the background information from the feature maps, *which can be regarded as the natural OOD samples*. However, a question arises: *How to design an OOD block sampler to select the positions representing background information from the feature maps?*

In Figure 3 (a), the ResNet-50 trained on ImageNet downsamples the input image and yields a corresponding feature map ( $\mathbb{R}^{H \times W \times C}$ ), where each image block is projected to a feature vector ( $\mathbb{R}^C$ ) located at the corresponding position. The classification head reports the category for each feature vector. We **highlight** the correctly classified blocks with over 40% confidence in Figure 3 (a) and (b). The results suggest that for blocks contained in the main objects, the confidence scores are much higher, while for the backgrounds far away from the main objects, their confidence scores are extremely low, *i.e.*, at least lower than 40%. *The confidence distribution on the feature map roots from the limited receptive fields of the cascaded convolution layers, i.e., each position of the feature map is only accessible to a local region of the input image*. Inspired by this observation, we posit the Self-supervised Sampling for OOD Detection (SSOD) based on the confidence score of each block.

#### 4.2 Formulation of SSOD

For a feature map within  $\mathbb{R}^{C \times H \times W}$  (*i.e.*, the channel, height, and width) produced by the neural networks, we can apply the classifier along spatial axes and obtain a confidence score map within  $\mathbb{R}^{M \times H \times W}$ , where  $M$  is the number of categories in ID data. The blocks with a low confidence score, *i.e.*, lower than 5%, on the ground-truth category, are recognized as OOD samples as **highlighted** in Figure 3 (c) and (d). Symmetrically, an ID block sampler selects some blocks with high confidence scores, *i.e.*, greater than 95%, as the ID samples (cf. Figure 3, the **green** blocks) besides the global average pooling feature, which helps to balance the positive (ID) and negative (OOD) samples.

Formally, we use  $h(\cdot)$ ,  $f_{cls}(\cdot)$ , and  $f_{ood}(\cdot)$  to denote the backbone removing the classification head, the multi-category classification head, and the binary ID/OOD discrimination head, respectively. Given an input image  $x$  with label  $y$ ,  $X^{C \times H \times W} = h(x)$  is the feature map. The prediction result of the classification model is:

$$\hat{y} = f_{cls}(\text{GAP}(h(x))) = f_{cls}(\text{GAP}(X^{C \times H \times W})), \quad (6)$$

where GAP is the global average pooling operation on the spatial dimensions. Similarly, when applying  $f_{cls}$  on each block of  $X^{C \times H \times W}$  without pooling operation, we can get the confidence score map  $\bar{y}^{M \times H \times W} = f_{cls}(X^{C \times H \times W})$  within  $\mathbb{R}^{M \times H \times W}$ . Moreover, we pick the confidence along



the target axis, *e.g.*, if the target label of  $x$  is  $j$ , then we collect the confidence along the  $j$ -th axis of  $M$ , yielding a target confidence map within  $\mathbb{R}^{H \times W}$ , *i.e.*,  $\bar{y}^{HW}$ . We use the ID/OOD sampler to select blocks with high/low scores on the target label as the ID/OOD supervision. Concretely, for  $i \in \{1, 2, 3, \dots, HW\}$ , we obtain the following self-supervised OOD labels from cls head:

$$y_i^{ood} = \begin{cases} 0, & \bar{y}_i^{HW} < 1 - \gamma \\ 1, & \bar{y}_i^{HW} \geq \gamma \\ \text{N/A}, & 1 - \gamma \leq \bar{y}_i^{HW} < \gamma \end{cases}, \quad (7)$$

where  $\bar{y}^{HW}$  indicates the predicted confidence of each image block belonging to the target category, and  $\gamma$  is a confidence threshold, *e.g.*, 95%. Remind that the image blocks assigned with the positive label are highlighted as **green** in Figure 3, and the negative blocks are marked using **red**. We drop the left image blocks (*i.e.*, N/A in Eqn.(7)), and therefore, they provide no ID/OOD signals during the training. With the OOD Head, we obtain the ID/OOD prediction ( $\hat{y}^{ood}$ ):

$$\hat{y}^{ood} = f_{ood}(X^{C \times H \times W}). \quad (8)$$

Since only a part of the image blocks is selected as ID/OOD supervision in Eqn.(7), consequently, the loss is performed on the corresponding predicted results in Eqn.(7) and Eqn.(8). The overall objective of SSOD is formulated with the cross entropy loss (CE):

$$\mathcal{L} = \text{CE}(\hat{y}, y) + \alpha \text{CE}(\hat{y}^{ood}, y^{ood}), \quad (9)$$

where  $\alpha$  is a balance parameter. During the training/inference phase, the OOD factor of input images can be calculated as follows:

$$P(x \in \mathcal{S}_{\mathbb{D}}) = \text{Sigmoid}(f_{ood}(\text{GAP}(X^{C \times H \times W}))), \quad (10)$$

where Sigmoid function is used to predict the probability of input image belonging to the ID data. With the proposed SSOD above, we can train the OOD detection branch end-to-end with realistic OOD supervisions sampled from the blocks of ID data as illustrated in Figure 1.

## 5 Experiments

We address the following problems in this section: 1) How does SSOD perform on OOD detection benchmarks? 2) Whether SSOD is stable under different hyper-parameter settings? 3) Whether SSOD is generalizable across different model architectures?

### 5.1 Experimental setup

We give a brief introduction of our employed datasets and the training parameters. The detailed information is attached in Appendix.

**Datasets.** We perform experiments on ImageNet [Russakovsky et al., 2015] and CIFAR-10 [Krizhevsky et al., 2009]. For ImageNet, we follow the settings from Sun et al. [2022] and employ iNaturalist [Horn et al., 2018], SUN [Xiao et al., 2010], Places [Zhou et al., 2018], and Textures [Cimpoi et al., 2014] as the OOD images. For CIFAR-10, we select SVHN [Netzer et al., 2011], LSUN [Yu et al., 2015], iSUN [Xu et al., 2015], Places, and Textures as the OOD images. Images in CIFAR-10 and ImageNet are resized and cropped to  $224 \times 224$ .

**Training and evaluation.** We use ResNet-50 [He et al., 2016] as our backbone and train in a total of 300 epochs. No complicated data augmentation schemes are used except for the RandomResizedCrop. The learning rate starts from  $1e-4$  and halves every 30 epochs. We optimize all parameters using the default gradient descent method.  $\alpha$  is set to 1.5 by default. We report the false positive rate of the OOD dataset when the true positive rate of ID images is 95%, *i.e.*, FPR95. We also provide the area under the receiver operating characteristic curve (AUROC) and classification accuracy of ID images (ID ACC) for comparison. We keep the quantity of ID/OOD data consistent.

**Selection of comparable techniques.** We choose both the classic and latest methods in dealing with OOD detection for comparisons. With regard to the classic schemes, we select the MSP [Hendrycks, 2017], MaDist [Lee et al., 2018b], ODIN [Liang et al., 2018], GODIN [Hsu et al., 2020], CSI [Tack et al., 2020], and MOS [Huang and Li, 2021]. Besides, we also use the Energy [Liu et al., 2020],

Table 1: OOD detection results on ImageNet.  $\downarrow$  indicates lower is better,  $\uparrow$  means greater is better. We highlight the best and second results using bold and underline.  $\Delta$  indicates the difference between SSOD and the best previous art, \* indicates our improvements. We use (w/) and (w/o) to indicate using and without using the supervised contrastive learning.

Method	<i>iNaturalist</i>		<i>SUN</i>		<i>Places</i>		$\uparrow$ ID ACC
	$\downarrow$ FPR95	$\uparrow$ AUROC	$\downarrow$ FPR95	$\uparrow$ AUROC	$\downarrow$ FPR95	$\uparrow$ AUROC	
MSP	54.99	87.74	70.83	80.86	73.99	79.76	<b>76.13</b>
MaDist	97.00	52.65	98.50	42.41	98.40	41.79	75.08
ODIN	<u>47.66</u>	89.66	60.15	84.59	67.89	81.78	75.08
GODIN	61.91	85.40	60.83	85.60	<u>63.70</u>	<u>83.81</u>	70.43
Energy	55.72	<u>89.95</u>	<u>59.26</u>	<u>85.89</u>	64.92	82.86	75.08
KNN (w/o)	59.08	86.20	69.53	80.10	77.09	74.87	75.08
<b>KNN (w/)</b>	<b>30.18</b>	<b>94.89</b>	<b>48.99</b>	<b>88.63</b>	<b>59.15</b>	<b>84.71</b>	<b>79.10</b>
SSOD (w/o)	<b>31.70</b>	<b>92.28</b>	<b>44.16</b>	<b>87.90</b>	<b>55.12</b>	<b>84.37</b>	<u>75.78</u>
<b>SSOD (w/)</b>	<b>20.32</b>	<b>95.28</b>	<b>35.52</b>	<b>92.06</b>	<b>41.44</b>	<b>89.38</b>	<b>75.12</b>
$\Delta$	15.96*	2.33*	15.10*	2.01*	8.58*	0.56*	0.35

which is the representative of the score-based calibration method, and the KNN [Sun et al., 2022], which is one of the latest schemes, as our comparable methods during the experiments. ResNet-18 and ResNet-50 [He et al., 2016] are chosen as the backbone of CIFAR-10 and ImageNet. SSOD employs the pre-trained ResNet-50 with a classification accuracy of 76.13% released by the official PyTorch community. We note that KNN [Sun et al., 2022] has two different versions, *i.e.*, w/ and w/o contrastive learning. For a fair comparison with other methods, we employ **no** contrastive learning tricks for all comparable techniques.

## 5.2 Comparisons with state-of-the-arts

We report the main results and answer the first question proposed at the beginning of Section.5, *i.e.*, the performance of SSOD on OOD benchmarks. After that, we analyze the failure cases of SSOD.

**OOD detection results on ImageNet.** We use natural images not included in ImageNet [Russakovsky et al., 2015] as the OOD set, such as iNaturalist [Horn et al., 2018], SUN [Xiao et al., 2010], and Places [Zhou et al., 2018]. We randomly select about 10k OOD images for each dataset following Sun et al. [2022]. All methods use **no** contrastive loss during the training. The detection results are shown in Table 1. A part of the results come from Sun et al. [2022].

From the results depicted in Table 1, we can notice that SSOD reduces the false positive rate (FPR95) over **13.21%** and improves the AUROC about **1.63%** on average. Specifically, on iNaturalist [Horn et al., 2018], which consists of natural landscape images, SSOD significantly reduces the FPR95 by over 15.96%, establishing the competitive state-of-the-art performance. Considering the Places [Zhou et al., 2018], which contains pictures such as the creek, field, and urban city, the objects included in these images have high similarity with that in ImageNet, and we argue that this phenomenon contributes to the lower improvements on this dataset. Consistently, the improvements of AUROC are also considerable on iNaturalist [Horn et al., 2018] and SUN [Xiao et al., 2010], evidencing the efficiency of our proposed SSOD.

**OOD detection results on CIFAR-10.** Since images appearing in CIFAR-10 [Krizhevsky et al., 2009] are smaller than that in ImageNet [Russakovsky et al., 2015], *i.e.*,  $32 \times 32$ , we use ResNet-18 [He et al., 2016] as the backbone for all comparable methods. Just as before, we use no contrastive loss during the training. Since SSOD extracts background information from the last feature maps and images in CIFAR-10 are too small, we resize the ID and OOD data to  $224 \times 224$  with RGB channels, yielding bigger feature maps. The experimental results are depicted in Table 2. The last column of Table 2 demonstrates the comparison between SSOD and the previous methods. We can notice that on OOD images such as SVHN [Netzer et al., 2011], LSUN [Yu et al., 2015], and iSUN [Xu et al., 2015], SSOD reports comparable performance as the best previous schemes with a marginal drop, *i.e.*, less than **4.06%**. On large-scale datasets such as Textures [Cimpoi et al., 2014] and Places [Zhou et al.,

Table 2: OOD detection results on CIFAR-10.  $\downarrow$  indicates lower is better,  $\uparrow$  means greater is better. We highlight the best and second results using bold and underline.  $\Delta$  is the difference between SSOD and the best previous art, \* indicates our improvements. All values are percentages.

OOD	Metrics	Methods								
		MSP	MaDist	ODIN	GODIN	Energy	CSI	KNN	SSOD	$\Delta$
<i>SVHN</i>	$\downarrow$ FPR95	59.66	<b>9.24</b>	20.93	15.51	54.41	37.38	24.53	<u>13.30</u>	4.06
	$\uparrow$ AUROC	91.25	<b>97.80</b>	95.55	96.60	91.22	94.69	95.96	<u>97.66</u>	0.14
<i>LSUN</i>	$\downarrow$ FPR95	45.21	67.73	7.26	<b>4.90</b>	10.19	<u>5.88</u>	25.29	7.51	2.61
	$\uparrow$ AUROC	93.80	73.61	98.53	<b>99.07</b>	98.05	<u>98.86</u>	95.69	98.72	0.35
<i>iSUN</i>	$\downarrow$ FPR95	54.57	<b>6.02</b>	33.17	34.03	27.52	10.36	25.55	<u>9.65</u>	3.63
	$\uparrow$ AUROC	92.12	<b>98.63</b>	94.65	94.94	95.59	98.01	95.26	<u>98.40</u>	0.23
<i>Textures</i>	$\downarrow$ FPR95	66.45	<u>23.21</u>	56.40	46.91	55.23	28.85	27.57	<b>14.39</b>	8.82*
	$\uparrow$ AUROC	88.50	92.91	86.21	89.69	89.37	<u>94.87</u>	94.71	<b>97.19</b>	2.32*
<i>Places</i>	$\downarrow$ FPR95	62.46	83.50	63.04	62.63	42.77	<u>38.31</u>	50.90	<b>17.63</b>	20.68*
	$\uparrow$ AUROC	88.64	83.50	86.57	87.31	91.02	<u>93.04</u>	89.14	<b>95.36</b>	2.32*
<i>Average</i>	$\downarrow$ FPR95	57.67	37.94	36.16	32.80	38.02	<u>24.20</u>	30.80	<b>12.50</b>	3.84*
	$\uparrow$ AUROC	90.90	89.29	92.30	93.52	93.05	<u>95.90</u>	94.15	<b>97.47</b>	0.78*
	$\uparrow$ ID ACC	<u>94.21</u>	<u>94.21</u>	<u>94.21</u>	93.96	<u>94.21</u>	<b>94.38</b>	<u>94.21</u>	93.91	0.30

2018], SSOD yields significant performance improvements compared to the current state-of-the-art techniques, specifically, reporting about **20.68%** performance gain (FPR95) on Places [Zhou et al., 2018]. Besides, with regard to the overall OOD detection ability, we can see that SSOD reduces the false positive rate over **3.84%** on the aforementioned five datasets on average and improves the AUROC about **0.78%**, which can be established as a new competitive OOD detection scheme.

**Analysis of the failure cases.** We tell the failure cases encountered by SSOD and point out its limitations. Recall that SSOD extracts OOD information from the background of training images and employs them as the proxy of OOD characters, revealing the potential of suffering limited diversity of the OOD supervision if the training images are not diverse. This phenomenon will be perceived if the OOD data is totally different in domains as the training images. For example, the training images are natural scenes, while the testing OOD data is synthetic color blocks or textures. To check this issue, We train the SSOD on ImageNet [Russakovsky et al., 2015] while testing it on Textures [Cimpoi et al., 2014]. From the results depicted in Table 3, though SSOD achieves top-ranked performance, it is worse than KNN [Sun et al., 2022], increasing the FPR95 by about 38.46%. This issue is caused by the overlap between ImageNet and Textures. Concretely, many images in the Textures carry vital symbols of objects included in ImageNet (cf. Figure 4). These overlaps lead to the inefficiency of SSOD during the comparison in Table 3.

### 5.3 Ablation Study

We tackle the last two problems posed at the beginning of this section, *i.e.*, the stability and scalability of our proposed SSOD.

**Ablations on the hyper-parameter  $\alpha$ .** Recall that  $\alpha$  controls the importance of loss generated by the OOD Head, balancing classifiers’ classification performance and OOD detection ability. We employ the CIFAR-10 [Krizhevsky et al., 2009] and Places [Zhou et al., 2018] as the ID and OOD data to validate the stability of  $\alpha$ . SSOD uses ResNet-18 as the backbone. From the ablations depicted in Table 4, we notice that with the increasing of  $\alpha$ , the classifier detects OOD input better, while the ID ACC is gradually descending. We expect to boost the robustness of classifiers while not affecting the model’s performance. Therefore, the  $\alpha$  equals 1.5 in our experiments.

**OOD detection across different model architectures.** We use ImageNet and Places as the ID and OOD data. Considering the deployment on portable devices, we test both the conventional and lite models, such as ResNet-50 [He et al., 2016], DenseNet-121 [Huang et al., 2017], RegNet (Y-800MF) [Radosavovic et al., 2020], and MobileNet [Howard et al., 2019]. Compared to Table 1, all methods shown in Table 6 achieve state-of-the-art performance, evidencing the scalability of SSOD.



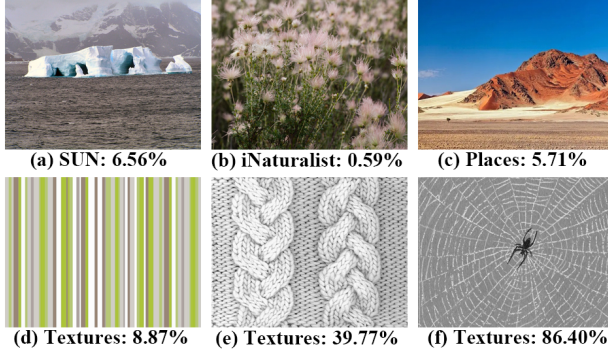


Figure 4: Confidence of OOD images assigned by SSOD. Successful cases: (a), (b), (c), and (d). These images are randomly sampled from several OOD dataset and assigned nominal ID confidence by the SSOD. Failure cases: (e) and (f). These images carry vital symbols of objects appearing in ImageNet, *e.g.*, (e) is the *braided* and (f) is *cobwebbed*, which are similar with the *knot* and *spider* in ImageNet.

**Imbalance issue between ID/OOD features.** During the training of the OOD head, we obtain much more background features since the objects only occupy a small part of the image. To promote training stability, we design three ways to tackle this issue, which are *Loss Weighting* (LW), *Data Resampling* (DR), and *Loss-Wise Balance* (LWB). LW multiplies a balance factor on the loss generated by the background features, DR samples equivalent ID/OOD features within each image, and LWB calculates the cross entropy generated by the ID/OOD features separately and picks their mean value as the loss objective. CIFAR-10 [Krizhevsky et al., 2009] and Places [Zhou et al., 2018] are the ID/OOD data. Based on the ablations depicted in Table 5, SSOD employs LWB for data balancing.

Table 4: Ablations on the hyper-parameter  $\alpha$ .

$\alpha$	0.7	1.0	1.5	1.8	2.0
$\downarrow$ FPR95	18.33	18.24	17.63	17.01	16.39
$\uparrow$ AUROC	94.62	94.97	95.76	95.82	96.09
$\uparrow$ ID ACC	94.00	93.91	93.91	92.10	91.17

Table 5: Ablations of balance schemes.

Scheme	LW	DR	LWB
$\downarrow$ FPR95	19.86	17.95	17.63
$\uparrow$ AUROC	93.13	95.44	95.36
$\uparrow$ ID ACC	92.74	94.00	93.91

Table 3: Failure cases on Textures. ImageNet [Russakovsky et al., 2015] is the training set and Textures [Cimpoi et al., 2014] is treated as the OOD data. No contrastive loss is used. The original copy of MOS [Huang and Li, 2021] tells no classification accuracy.

Methods	Textures	
	$\downarrow$ FPR95	$\uparrow$ AUROC
MSP	68.00	79.61
MaDist	55.80	85.01
ODIN	50.23	85.62
GODIN	77.85	73.27
MOS	60.43	81.23
KNN	<b>11.56</b>	<b>97.18</b>
SSOD	<u>50.02</u>	<u>86.11</u>

Table 6: Ablations of different model architectures. R-50, D-121, Reg, and Mobile indicate ResNet-50, DenseNet-121, RegNet, and MobileNet, respectively.  $\times$  represents the vanilla counterpart, while  $\checkmark$  is the SSOD version.

Model	R-50	D-121	Reg	Mobile
$\downarrow$ FPR95 ( $\times$ )	73.99	68.75	71.66	73.27
$\downarrow$ FPR95 ( $\checkmark$ )	57.24	51.39	50.48	54.37
$\triangle$	16.75*	17.36*	21.18*	18.90*

## 6 Conclusion and discussion

This paper proposes a probabilistic framework that divides the OOD detection problem into two factors, *i.e.*, ID and OOD factors. This provides a comprehensive overview of existing OOD methods and highlights the critical constraint of relying on pre-trained features. To address this limitation, we introduce an end-to-end scheme called SSOD which trains the OOD detection objective jointly with the ID classification. This approach leverages OOD supervision from the background information of ID images, eliminating the need for additional costs. Extensive experiments have validated that SSOD achieves state-of-the-art performance in detecting OOD data.

To the best of our knowledge, SSOD is the first method that generates natural OOD supervision to unlock the potential of the end-to-end paradigm. However, SSOD is based on the local property from convolutions, which are not applied for transformers built with cascaded attention and FFN layers, *e.g.*, ViT. Thus, discovering a more general self-supervised OOD sampler for different network architectures is a valuable and necessary direction.

## References

- Haoyue Bai, Fengwei Zhou, Lanqing Hong, Nanyang Ye, S.-H. Gary Chan, and Zhenguo Li. Nas-ood: Neural architecture search for out-of-distribution generalization. In *ICCV*, 2021.
- Nicolas Carion, Francisco Massa, Gabriel Synnaeve, Nicolas Usunier, Alexander Kirillov, and Sergey Zagoruyko. End-to-end object detection with transformers. In *ECCV*, 2020.
- Minghui Chen, Cheng Wen, Feng Zheng, Fengxiang He, and Ling Shao. VITA: A multi-source vicinal transfer augmentation method for out-of-distribution generalization. In *AAAI*, 2022.
- Mircea Cimpoi, Subhansu Maji, Iasonas Kokkinos, Sammy Mohamed, and Andrea Vedaldi. Describing textures in the wild. In *CVPR*, 2014.
- Patrick Dendorfer, Sven Elflein, and Laura Leal-Taixé. Mg-gan: A multi-generator model preventing out-of-distribution samples in pedestrian trajectory prediction. In *ICCV*, 2021.
- Xuefeng Du, Zhaoning Wang, Mu Cai, and Yixuan Li. VOS: learning what you don’t know by virtual outlier synthesis. In *ICLR*, 2022.
- Kaiming He, Xiangyu Zhang, Shaoqing Ren, and Jian Sun. Deep residual learning for image recognition. In *CVPR*, 2016.
- Dan Hendrycks. A baseline for detecting misclassified and out-of-distribution examples in neural networks. In *ICLR*, 2017.
- Grant Van Horn, Oisin Mac Aodha, Yang Song, Yin Cui, Chen Sun, Alexander Shepard, Hartwig Adam, Pietro Perona, and Serge J. Belongie. The inaturalist species classification and detection dataset. In *CVPR*, 2018.
- Andrew Howard, Ruoming Pang, Hartwig Adam, Quoc V. Le, Mark Sandler, Bo Chen, Weijun Wang, Liang-Chieh Chen, Mingxing Tan, Grace Chu, Vijay Vasudevan, and Yukun Zhu. Searching for mobilenetv3. In *ICCV*, 2019.
- Yen-Chang Hsu, Yilin Shen, Hongxia Jin, and Zsolt Kira. Generalized ODIN: detecting out-of-distribution image without learning from out-of-distribution data. In *CVPR*, 2020.
- Gao Huang, Zhuang Liu, Laurens van der Maaten, and Kilian Q. Weinberger. Densely connected convolutional networks. In *CVPR*, 2017.
- Rui Huang and Yixuan Li. Mos: Towards scaling out-of-distribution detection for large semantic space. In *CVPR*, 2021.
- Rui Huang, Andrew Geng, and Yixuan Li. On the importance of gradients for detecting distributional shifts in the wild. In *NeurIPS*, 2021.
- Alex Krizhevsky, Geoffrey Hinton, et al. Learning multiple layers of features from tiny images. 2009.
- Kimin Lee, Honglak Lee, Kibok Lee, and Jinwoo Shin. Training confidence-calibrated classifiers for detecting out-of distribution samples. In *ICLR*, 2018a.
- Kimin Lee, Kibok Lee, Honglak Lee, and Jinwoo Shin. A simple unified framework for detecting out-of-distribution samples and adversarial attacks. In *NeurIPS*, 2018b.
- Shiyu Liang, Yixuan Li, and R. Srikant. Enhancing the reliability of out-of-distribution image detection in neural networks. In *ICLR*, 2018.
- Weitang Liu, Xiaoyun Wang, John D. Owens, and Yixuan Li. Energy-based out-of-distribution detection. In *NeurIPS*, 2020.
- Yifei Ming, Yiyu Sun, Ousmane Dia, and Yixuan Li. How to exploit hyperspherical embeddings for out-of-distribution detection? In *ICLR*, 2023.
- Felix Möller, Diego Botache, Denis Huseljic, Florian Heidecker, Maarten Bieshaar, and Bernhard Sick. Out-of-distribution detection and generation using soft brownian offset sampling and autoencoders. In *CVPR Workshops*, 2021.

- Yuval Netzer, Tao Wang, Adam Coates, Alessandro Bissacco, Bo Wu, and Andrew Y Ng. Reading digits in natural images with unsupervised feature learning. In *NeurIPS Workshops*, 2011.
- Sen Pei, Xin Zhang, Richard YiDa Xu, Bin Fan, and Gaofeng Meng. Out-of-distribution detection with boundary aware learning. In *ECCV*, 2022.
- Ilija Radosavovic, Raj Prateek Kosaraju, Ross B. Girshick, Kaiming He, and Piotr Dollár. Designing network design spaces. In *CVPR*, 2020.
- Joseph Redmon, Santosh Kumar Divvala, Ross B. Girshick, and Ali Farhadi. You only look once: Unified, real-time object detection. In *CVPR*, 2016.
- Olga Russakovsky, Jia Deng, Hao Su, Jonathan Krause, Sanjeev Satheesh, Sean Ma, Zhiheng Huang, Andrej Karpathy, Aditya Khosla, Michael Bernstein, Alexander C. Berg, and Li Fei-Fei. ImageNet Large Scale Visual Recognition Challenge. In *IJCV*, 2015.
- Yiyu Sun, Chuan Guo, and Yixuan Li. React: Out-of-distribution detection with rectified activations. In *NeurIPS*, 2021.
- Yiyu Sun, Yifei Ming, Xiaojin Zhu, and Yixuan Li. Out-of-distribution detection with deep nearest neighbors. In *ICML*, 2022.
- Jihoon Tack, Sangwoo Mo, Jongheon Jeong, and Jinwoo Shin. CSI: novelty detection via contrastive learning on distributionally shifted instances. In *NeurIPS*, 2020.
- Keke Tang, Dingrui Miao, Weilong Peng, Jianpeng Wu, Yawen Shi, Zhaoquan Gu, Zhihong Tian, and Wenping Wang. Codes: Chamfer out-of-distribution examples against overconfidence issue. In *ICCV*, 2021.
- Hongxin Wei, Renchunzi Xie, Hao Cheng, Lei Feng, Bo An, and Yixuan Li. Mitigating neural network overconfidence with logit normalization. In *ICML*, 2022.
- Jianxiong Xiao, James Hays, Krista A. Ehinger, Aude Oliva, and Antonio Torralba. SUN database: Large-scale scene recognition from abbey to zoo. In *CVPR*, 2010.
- Pingmei Xu, Krista A. Ehinger, Yinda Zhang, Adam Finkelstein, Sanjeev R. Kulkarni, and Jianxiong Xiao. Turkergaze: Crowdsourcing saliency with webcam based eye tracking. 2015.
- Fisher Yu, Yinda Zhang, Shuran Song, Ari Seff, and Jianxiong Xiao. LSUN: construction of a large-scale image dataset using deep learning with humans in the loop. 2015.
- Bolei Zhou, Àgata Lapedriza, Aditya Khosla, Aude Oliva, and Antonio Torralba. Places: A 10 million image database for scene recognition. 2018.

## A Dataset

We introduce the details of datasets in this section.

**ImageNet.** ImageNet [Russakovsky et al., 2015] is well known in image classification problems, containing 1000 classes from the natural scene such as *tiger*, *goldfish*, *house*, to name a few. This dataset is usually used as the in-distribution data, expecting to get higher confidence from the classifier.

**CIFAR-10.** CIFAR-10 [Krizhevsky et al., 2009] is smaller compared to the ImageNet. It consists of tiny images within 10 classes, such as *airplane*, *bird*, *dog*, *etc.* All images contained in CIFAR-10 are in the shape of  $32 \times 32$ . In our experiments, we treat CIFAR-10 as the in-distribution data and resize images into  $224 \times 224$  to get bigger feature maps. Noting that this operation introduces no significant influence on the classification performance.

**SVHN.** The full name of SVHN [Netzer et al., 2011] is the street view house number, consisting of digit numbers from the natural street view. Following Sun et al. [2022], we randomly select 10k images from this dataset to serve as the out-of-distribution data. All pictures from OOD data are expected to get lower confidence from the classifier.

**LSUN.** This dataset is used for visual recognition, which was presented by Yu et al. [2015]. It consists of over one million labeled images, including 10 scene and 20 object categories. Following Sun et al. [2022], 10k images from LSUN are treated as the OOD data.

**iNaturalist.** The existing dataset in the image classification problem usually has a uniform distribution across different objects and categories. However, in the real world, the images could be heavily imbalanced. To bridge this gap between experimental and practical settings, iNaturalist [Horn et al., 2018], consisting of over 859k images within about 5k species (*i.e.*, planets and animals), is presented. We randomly select 10k images from this dataset to serve as the OOD pictures.

**iSUN.** This dataset is constructed based on the SUN [Xiao et al., 2010]. iSUN [Xu et al., 2015] is a standard dataset for scene understanding, containing over 20k images from SUN database. We use 10k iSUN images as the OOD data.

**Textures.** This dataset consists of images carrying vital characters, *i.e.*, patterns and textures, of natural objects. Presented in Cimpoi et al. [2014], Textures aims at supporting the analytical dimension in image understanding. In our experiments, we treat Textures as the OOD data.

**Places.** This dataset is used for scene recognition which was presented by Zhou et al. [2018], including over 10 million images such as *badlands*, *bamboo forest*, *canal*, and *etc.* We use a part, *i.e.*, 10k, of these images from Sun et al. [2022] to play the role of OOD data.

## B Training Details

All images used in our experiments are resized to  $224 \times 224$ . We just use simple data transformations, such as RandomResizedCrop and Normalization. We use AdamW as the default optimizer. The learning rate starts from  $1e-4$  and halves every 30 epochs. The experiment runs on 8 Nvidia Tesla V100<sup>3</sup> GPUs using distributed training pipeline of PyTorch<sup>4</sup>. The batch size is set to 256, *i.e.*,  $32 \times 8$ . No complicated tricks are used during the training and inference phases. We store the checkpoints yielding the best FPR95 performance. For more details about the training and architectures, please refer to our attached source codes in the *Supplementary Material*.

---

<sup>3</sup><https://www.nvidia.com/en-us/data-center/v100/>

<sup>4</sup><https://pytorch.org/>